Uranium dioxides and debris fragments released to the environment with cesium-rich microparticles from the Fukushima Daiichi Nuclear Power Plant

DOI:
10.1021/acs.est.7b06309

Document Version
Accepted author manuscript

Published in:
Environmental Science and Technology

Uranium dioxides and debris fragments released to the environment with cesium-rich microparticles from the Fukushima Daiichi Nuclear Power Plant

Asumi Ochiai,[1] Junpei Imoto,[1] Mizuki Suetake,[1] Tatsuki Komiya,[1] Genki Furuki,[1] Ryohei Ikehara,[1] Shinya Yamasaki,[2] Gareth T. W. Law,[3] Toshihiko Ohnuki,[4] Bernd Grambow,[5] Rodney C. Ewing,[6] Satoshi Utsunomiya[*,1]*

[1]Department of Chemistry, Kyushu University, 744 Motooka, Nishi-ku, Fukuoka 819-0395, Japan

[2]Faculty of Pure and Applied Sciences and Center for Research in Isotopes and Environmental Dynamics, University of Tsukuba, 1-1-1 Tennodai, Tsukuba, Ibaraki 305-8577, Japan

[3]Centre for Radiochemistry Research, School of Chemistry, The University of Manchester, Oxford Road, Manchester, M13 9PL UK

[4]Laboratory for Advanced Nuclear Energy, Institute of Innovative Research, Tokyo Institute of Technology, 2-12-1 Ookayama, Meguro-ku, Tokyo 152-8550, Japan

[5]SUBATECH, IMT Atlantique, CNRS-IN2P3, the University of Nantes, Nantes 44307, France

16 [6]Department of Geological Sciences and Center for International Security and Cooperation,
17 Stanford University, Stanford, CA 94305-2115 USA

18

19 **Abstract**

20 Trace U was released from the Fukushima Daiichi Nuclear Power Plant (FDNPP) during the
21 meltdowns, but the speciation of the released components of the nuclear fuel remains unknown.
22 We report, for the first time, the atomic-scale characteristics of nano-fragments of the nuclear
23 fuels that were released from the FDNPP into the environment. Nano-fragments of an intrinsic
24 U-phase were discovered to be closely associated with radioactive cesium-rich microparticles
25 (CsMPs) in paddy soils collected ~4 km from the FDNPP. The nano-scale fuel fragments were
26 either encapsulated by or attached to the CsMPs and occurred in two different forms: (*i*) UO_{2+X}
27 nanocrystals of ~70 nm size, which are embedded into magnetite associated with Tc and Mo on
28 the surface. (*ii*) Isometric $(U,Zr)O_{2+X}$ nanocrystals of ~200 nm size, with the U/(U+Zr) molar
29 ratio ranging from 0.14 to 0.91, with intrinsic pores (~6 nm), indicating the entrapment of vapors
30 or fission-product gasses during crystallization. These results document the heterogeneous
31 physical and chemical properties of debris at the nanoscale, which is a mixture of melted fuel
32 and reactor materials, reflecting the complex thermal processes within the FDNPP reactor during
33 meltdown. Still the CsMPs are an important medium for the transport of debris fragments into
34 the environment in a respirable form.

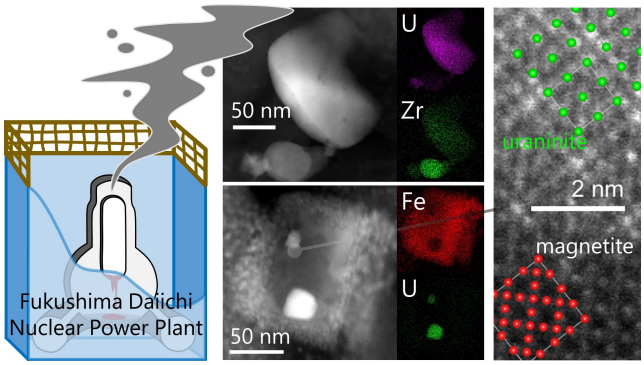

Introduction

The nuclear disaster at the Fukushima Daiichi Nuclear Power Plant (FDNPP) in March 2011 released ~5.2×10^{17} becquerels (Bq) of fission products and actinides into the environment.[1] At present, the principal contributions to radiation dose in the surrounding environment are derived from ^{134}Cs and ^{137}Cs because of their half-lives (2.065 and 30.17 years, respectively), their high mobility in the atmospheric environment, and the large released activity (~10^{16} Bq of ^{134}Cs and ^{137}Cs).[1,2] Although soluble species such as CsOH and CsI are typically reported as Cs phases in the severe accidents with irradiated fuels,[3] sparingly soluble Cs-rich micro-particles (CsMPs) that mainly comprise Si-glass and Fe-Zn-Cs nanoparticles have been recently identified as an unexpected chemical form of Cs released from the FDNPP.[4,5] The CsMPs are considered to form through the condensation of SiO(g) vaporized through molten corium-concrete interaction (MCCI), in which the melted nuclear fuel abruptly reacts with the concrete pedestal of the nuclear reactor primary-containment vessel (PCV).[5,6]

The CsMPs have been occasionally found associated with trace U.[7,8] Further detailed characterization revealed that in some cases the U occurs associated with Fe-Zn nanoparticles as

small as ~10 nm without forming crystalline phases.[5] In these instances the U concentration is very low (~1 wt% at maximum), indicating the adsorption of U oxides, volatilized at > ~1,900 K from partially oxidized uranium dioxide.[5,9,10] Although the total amount of U released from the FDNPP, estimated from limited data as 3.9×10^6 Bq,[11] may be ten orders of magnitude lower than the total released Cs radioactivity, acquiring knowledge on the released U is important in order to understand the environmental impact of the FDNPP accident, and to provide much needed data on the status of the melted nuclear fuels in the damaged reactors, of which the mixture with structural materials is called "debris." At present, the decommissioning of the damaged FDNPP reactors is the most challenging operation at the site because of the high radiation fields inside the reactors (~ 80 Sv/h at Unit 2 on March 17, 2017 as determined by Tokyo Electric Power Company (TEPCO)) and resulting lack of data.[12] Thus, the more information on the physical and chemical properties of the fuel the better, as it is essential for the removal and future management of the debris. Fragments of nuclear fuels bearing U, other actinides, and fission products, which have not been found to date in Fukushima, are also known to be an important medium for influencing the mobility and bioavailability of radionuclides after nuclear accidents.[13,14] In turn, they influence impact and risk assessments.[15] Further, the fragment particles are the only direct evidence to provide information on the physical and chemical properties of real debris remaining inside the damaged reactors. The present study reports, for the first time, direct observation of nano-sized "debris fragments" released from the FDNPP based on the detailed atomic-resolution analysis in order to further elucidate their formation processes and partially assess their chemical properties.

Materials and Methods

Sampling

The sampling campaign was conducted at two locations on March 16, 2012. Surface soils were collected from the top ~1 cm of soil at an aquaculture center (AQC) and Ottozawa (OTZ) located ~2 km south and ~4 km west of the FDNPP in Okuma Town, Futaba County, Fukushima, respectively. See map in Furuki et al.[5] Six soils were collected from a side ditch at AQC and 15 soils were collected a paddy field at QTZ. The soils were primarily composed of clay minerals, quartz and feldspars. Three CsMPs were separated from the soils: one from AQC and two from OTZ. The CsMPs were labeled as AQC-A, OTZ-A, and OTZ-B, which correspond to AQC2, OTZ6, and OTZ9, respectively, in the Kyushu University CsMP archive.

Isolation of CsMPs

The procedure for separating CsMPs from soil samples follows that outlined in our previous study.[5] Initially, the soil samples were sieved through a 114-μm mesh. The powder samples were dispersed on grid paper and covered with a plastic sheet; an imaging plate (IP, Fuji film, BAS-SR 2025) was then placed on the samples for 5-25 minutes. The autoradiograph image was recorded with a pixel size of 50-100 μm using an IP reader. After identifying the positions of intense radioactive spots, droplets of pure water were added to these positions and then drawn using a pipette to make a suspension with a small amount of soil particles. The procedure was repeated until the suspension did not contain a significant amount of soil particles.

Thereafter, using double-sided carbon tape, the position containing a hot spot was sampled. The section containing the hot particle was cut as small as possible using a blade, and the pieces were checked by autoradiograph imaging, so that scanning electron microscopy (SEM) observation could be performed to locate the CsMPs with maximum efficiency. The pieces were placed on an

aluminum plate and coated with carbon using a carbon coater (SANYU, SC-701C) prior to SEM analysis. The CsMP was found using an SEM (Shimadzu, SS550 and Hitachi, SU6600) equipped with energy dispersive X-ray spectrometry (EDX, EDAX Genesis). The acceleration voltage was 5-25 kV for imaging details of the surface morphology and 15-25 kV for elemental analysis, including area analysis and elemental mapping.

Preparation of the TEM specimen

A focused ion beam (FIB) system (FEI, Quanta 3D FEG 200i Dual Beam) was utilized to prepare thin foils of individual CsMPs with diameters of a few μm. The ion source was Ga, while W deposition was used to minimize damage by the ion bombardment. The current and acceleration voltage of the ion beam were adjusted to be 100 pA to 30 nA and 5–30 kV depending on the progress of thinning and sample properties such as hardness and size. The thinned piece was attached to the semilunar-shaped Cu grid for FIB and further thinned by an ion beam at 5 kV.

Transmission electron microscopy (TEM) analysis

High-resolution TEM (HRTEM) with energy dispersive X-ray analysis (EDX) and high-angle annular dark-field scanning transmission electron microscopy (HAADF-STEM) were performed using JEOL JEM-ARM200F and JEM-ARM200CF with an acceleration voltage of 200 kV. The JEOL Analysis Station software and Thermo Scientific NSS software were used to control the STEM-EDX mapping. To minimize the effect of sample drift, a drift-correction mode was used during acquisition of the elemental map. The STEM probe size was ~0.13 nm, generating ~140 pA of current when 40 μm of the condenser lens aperture was inserted. The collection angle of the HAADF detector was ~97–256 mrad.

Three dimensional visualization utilizing STEM tomography

The 3D tomography of the Fe-U particle in OTZ-A was performed in HAADF-STEM image mode using a JEOL JEM-ARM200CF. The HAADF-STEM images were acquired by tilting from -70° to +69° at intervals of 1°. ImageJ (NIH), TEMography™ (SYSTEM IN FRONTIER), and Amira (Maxnet) were used to reconstruct the 3D structure.

Gamma spectrometry

The ^{134}Cs and ^{137}Cs radioactivities of the CsMPs were determined using gamma spectrometry. The radioactivity of an additional micro-particle with a size of ~400 μm obtained from the surface soil in Fukushima was precisely determined at the radioisotope center in Tsukuba University, Japan, and utilized as a standard point specimen for ^{134}Cs and ^{137}Cs. The radioactivity of the point source standard was 23.9 Bq for ^{134}Cs and 94.6 Bq for ^{137}Cs as of September 29, 2015. The measurement of radioactivity was performed on the CsMPs and the point source standard using Ge semi-conductor detectors GMX23 (SEIKO E&G) and GX6020 (Canberra) at the Center for Radioisotopes in Kyushu University, Japan. The acquisition times were: 83121 s for AQC-A using GMX23; 87481 s for OTZ-B using GMX23; and 70000 s for OTZ-A using GX6020.

Results

In the present study, uranium oxide nanoparticles were discovered to be associated with three CsMPs that were separated from soils collected within ~4 km of the FDNPP; at an aquaculture center (AQC) and Ottozawa (OTZ).[5] It is extremely difficult to find isolated uranium oxide

nanoparticle in the environment surrounding the FDNPP. In the present study, the CsMP was a key to the discovery of uranium oxide nanoparticles. The CsMPs are designated as AQC-A, OTZ-A and OTZ-B. The radioactivity of the CsMPs and other relevant parameters are summarized in Table S1. The $^{134}Cs/^{137}Cs$ activity ratios were determined to be 0.98-1.07, which approximately corresponds to the burnup calculated for the reactors at the FDNPP.[16] Scanning electron microscopy energy dispersive X-ray analysis (SEM-EDX) revealed that all CsMPs are mainly composed of Si, Fe, Zn and Cs (Figure 1).

OTZ-A

OTZ-A contains 7.4-34.5 wt% of Cs (as Cs_2O) as determined by STEM-EDX standardless analysis (Table S2 and Figure S1A). In addition to large angular pores and some inclusions, OTZ-A contained a Fe-oxide nanoparticle of ~100 nm size, which was attached to the CsMP surface (indicated by the white square in Figure 2A). A discrete U phase was observed within the Fe-oxide nanoparticle (Figure S1B). HAADF-STEM and HRTEM images of the same Fe-oxide nanoparticle, further thinned by FIB, revealed the presence of two U-oxide nanoparticles of ~10 nm and ~30 nm size (Figure 2B, S2A, and S2C). These textures were not created by electron beam irradiation during TEM observation but rather represent the original phases because the radiation-induced formation of U-oxide nanocrystals requires much higher doses than that used in this study.[17] Based on the atomic-resolution HAADF-STEM and the selected area electron diffraction (SAED) pattern, the Fe-oxide and U-oxide nanoparticles were identified to be magnetite (Fe_3O_4) and uraninite (UO_{2+X}), respectively (Figure 2C and the SAED viewed from the other zone axis in Figure S2B). The two SAEDs explicitly reveal that these two phases are oriented with same zone axes, indicating the structural relation of epitaxial growth between magnetite and uraninite (Figure 2D). High-resolution HAADF-STEM with atomic-resolution

STEM elemental maps clearly show an array of U atoms within the uraninite nanoparticle and arrayed Fe atoms in the same direction. The HR-HAADF-STEM image (Figure 2C) displays enhanced contrast at every 4 or 5 atomic columns, both in *a* and *b* axes within the portion of the U-oxide nanoparticle. This is due to the over- or under-lying Fe atoms in the same orientation along the projected zone axis, because magnetite and uraninite are both isometric with unit cell parameters of 0.83958 nm[18] and 0.54682 nm[19], respectively.

The three dimensional electron tomography of the magnetite nanoparticle also revealed the presence of two euhedral uraninite nanocrystals completely enclosed in a part of euhedral magnetite crystal oriented toward the same direction, which is consistent with crystallographic relation of epitaxial growth (Figure 2E and 2F, and movie S1). The magnetite nanoparticle is also associated with trace concentrations of Tc and Mo as revealed by the EDX analyses (Figure S2D). The line scan analysis of a traverse of the further thinned specimen reveals that Tc and Mo are present on the exterior of the magnetite nanoparticle (Figure 2G). Hence, the magnetite containing the uraninite nanoparticles formed without impurities that can be detected by EDX (~0.1 wt%), and Tc and Mo were subsequently adsorbed to the surface. The Tc association should have occurred inside the reactors, because the Tc concentration is diluted when dispersed to the environment. Because Tc isotopes scarcely occur naturally but are generated as a fission product in nuclear reactor,[20] the Tc occurrence over the surface of the magnetite nanocrystal provides strong evidence that the uraninite nanocrystals embedded in magnetite nanocrystal originated inside the reactors. Thus, it is identified as nanoscale fragment of reactor debris.

AQC-A

Figure 3A shows a HAADF-STEM image of the cross-section of AQC-A, displaying domains with high Cs concentration (high contrast at the area 1) (Table S2) in a porous matrix that has lower Cs concentrations (represented by area 5). The texture is indicative of aggregation of individual dense CsMP particles. Within the porous portion of the CsMP, a euhedral Fe-oxide nanocrystal of ~400 nm size was found, which also had an embedded uranium dioxide nanoparticle of ~70 nm size (Figure 3B). This U oxide nanoparticle had a similar shape, composition, and host phase as those characterized in OTZ-A. It is important to note that this TEM specimen was prepared by FIB and the TEM image shows the cross section of the CsMP. Thus, the Fe-oxide containing uraninite nanoparticle is encapsulated in the CsMP. Because the CsMP formed inside the reactors, the Fe-oxide nanoparticle with the embedded U-oxide nanoparticle originated from the reactors as well, indicating that the nanoparticles are nano-fragments of reactor debris as well as the one found in OTZ-A.

OTZ-B

OTZ-B occurs as an aggregate of at least three spherical CsMPs each of ~1 μm size (Figure 4A), and their compositions were determined to be 2.8-32.2 wt% of Cs_2O, 9.1-26.1 wt% of Fe_2O_3, 0.0-7.3 wt% of ZnO, and 45.6-73.7 wt% of SiO_2 (Figure S3 and Table S2). This is consistent with the composition of CsMPs described in the literature.[5,9] Notably, eleven U–Zr-oxides nanoparticles were found within this aggregate (Figure 4A and B). All of the U-Zr particles were characterized as solid solutions as revealed by the magnified image and the elemental maps (Figure 4C). See SI (page S7) for further information on the identification of solid solution. Further, the Zr and U distribution are almost homogeneous within the individual grains. The molar fraction of U in the U–Zr-oxides, U/(U+Zr), determined by STEM-EDX analysis, varied widely between the particles, ranging from 0.14 to 0.91 (Figure 4D).

After further thinning of OTZ-B by FIB, the U–Zr-oxides nanoparticles labelled as 1 and 2 (Figure 4C and E) were identified to be uraninite and cubic zirconia based on the SAED patterns, respectively. Note, the extra diffraction maxima, which are absent due to an extinction rule in the cubic structure, e.g., 210 and 120, appeared in the pattern because of the substitution of U atoms in the solid solution as shown by the simulated diffraction pattern for cubic ZrO_2 with 25% substitution of U for Zr (Figure S4). High-resolution HAADF-STEM images and the SAED patterns reveal that both particles are single crystals (Figure 4E) and that particle 1 has pores of ~6 nm diameter (Figure S5A and B) and a few defects (Figure S5B-E). The U/(U+Zr) molar ratios are 0.91 for particle 1 and 0.17 for particle 2, indicating that U–Zr-oxide solid solution can form with a large variation in the mixing ratio. In addition, similar to OTZ-A, Tc occurrence was observed in Fe-rich areas (Figure S6), providing further indication that the CsMP and the U–Zr-oxide nanoparticles are derived from the FDNPP.

Discussion

Formation processes of the reactor debris fragments

The U nanoparticles and the Fe-oxide nanoparticles in AQC-A and OTZ-A have uraninite (UO_{2+X}), $X < 0.33$ and magnetite structures, respectively, with octahedral crystalline shape. The Fe source for the magnetite was likely the stainless steel of the reactor pressure vessel (RPV) and/or other metal parts of the fuel assembly. The chemical form of Fe has been considered to be metallic in the fuel debris at the FDNPP based on the severe accident analysis calculations,[21,22] though magnetite (Fe_3O_4) particles were characterized in the present study. The molten Fe metal can slightly vaporize above the melting temperature, 1811 K,[23] and the vaporized Fe can easily

bond to oxygen to form Fe-oxide nanoparticles, mainly magnetite.[24] However, the vaporization/condensation mechanism may not account for all of the formed magnetite, because the shape of the magnetite nanoparticles produced through vaporization/condensation processes in welding fumes are generally spherical,[25,26] which is clearly different from the octahedral shape observed in OTZ-A and AQC-A. Rather, their octahedral morphology indicates a slower crystallization processes similar to the euhedral ferrous particles and uraninite nanoparticles found in the Three Mile Island reactor unit 2 (TMI-2).[27,28] The occurrence of epitaxially grown magnetite indicates that a part of Fe metal was oxidized before crystallization over the uraninite nanocrystals. That is, the epitaxial growth of magnetite over uraninite excludes the possibility of the initial formation of Fe metal over the uraninite nanoparticles. Considering the large difference in the melting points of magnetite and UO_{2+X}; 1863 K and 2900 K, respectively,[27] the solidification of uraninite nanocrystals would first proceed within the Fe oxides melts as its cools, followed by the epitaxial growth of magnetite over uraninite nanocrystals.

The U–Zr-oxide nanoparticles in OTZ-B likely formed from a U–Zr-oxide melt, which would have resulted from the interaction of molten fuel and ZrO_2 that had previously been produced through the reaction of zircalloy and steam at high temperature > ~1500 K.[6] The liquidus temperature of U–Zr oxides is as high as ~2800–3000 K depending on the Zr fraction,[29] which is, in general, slightly lower than the melting points of pure UO_{2+X} and ZrO_2, 2900 K and 2960 K, respectively.[27] This indicates that the particle was locally heated higher than ~2800 K. The melting temperature can be even lower than 2800 K in corium, which is a lava-like melt of the fuels, because the liquidus and solidus temperatures of the hyperstoichiometric U oxides (up to $UO_{2.21}$) decrease to as low as 2800 K and 2400 K, respectively.[30] In addition, the wide range in the composition of U–Zr oxides (U/(U+Zr) = 0.14–0.91), indicates that the melt did not form a

252 large-scale pool of homogeneous composition. Rather, the U–Zr-oxide eutectic occurred
253 heterogeneously at the micron scale due to spatial variations in the chemistry.

254 According to the U–Zr–O phase diagram, when the melt composition is close to the ZrO_2 end-
255 member (U/(U+Zr) = 0.14), the cubic phase is stable below the solidus temperature, and there is
256 a structural transition from cubic to tetragonal at ~2400 K (2620 K in case of stoichiometric
257 zirconia) when cooled down.[31,32] Although the cubic phase is stable only above ~2400 K in the
258 phase diagram, the U–Zr oxides retained the cubic structure at ambient temperature in OTZ-B,
259 most likely because of rapid cooling of the liquid U–Zr-oxides droplets. In case of the TMI-2, U–
260 Zr oxide was reported to be tetragonal rather than monoclinic, which is stable at <1300 K also
261 because of the rapid cooling process.[32] The cubic U–Zr-oxide nanoparticles identified in the
262 present study probably formed by a more rapid cooling process than that which occurred at TMI-
263 2.

264 From these data, part of the process that the FDNPP fuels experienced during the meltdown can
265 be summarized as the follows: Cooling waters vaporized and the steam reacted with Zr and Fe
266 forming their oxides after the loss of power to the cooling system; UO_2, which is the main
267 composition of fuels, partially oxidized and volatilized at > ~1,900 K.[9,10] The fuel assemblies
268 melted unevenly with relatively less-irradiated fuels being heated to a higher temperature as
269 compared with the high burn-up fuels and volatilized as evidenced by the $^{235}U/^{238}U$ isotopic
270 ratio.[9] The fuel assembly collapsed and moved to the bottom of RPV. The temperature increased
271 locally to at least >2400 K based on the liquidus temperature of U–Zr-oxides. Locally-formed
272 oxides melted to a heterogeneous composition, including a small amount of the Fe oxides,[27]
273 which then became a source of Fe–U-single crystals and U–Zr-oxide eutectic phases.
274 Specifically, euhedral magnetite nanocrystals encapsulated euhedral uraninite nanocrystals,

which would have crystallized slowly at this stage. Liquid U–Zr-oxides nano-droplets were rapidly cooled and solidified to a cubic structure. When the molten fuels hit the concrete pedestal of the primary containment vessel (PCV), SiO gas was generated at the interfaces between the melted core and concrete, and instantly condensed to form CsMPs.[5] The U–Zr-oxide nanoparticles or the magnetite nanocrystals subsequently formed aggregates with CsMPs. Finally, the reactor debris fragments were released to the environment along with CsMPs.

Insights into the current status of debris properties

Grambow and Poinssot[33] have discussed the possible composition of corium, the risk, and its stability in the damaged reactors at the FDNPP. In general, the amounts of fission products and U remaining in the corium strongly depend on their volatility, which were classified into volatile (Cs, I), semi-volatile (Ba, Tc, Mo), low volatility (Sr, La), and nonvolatile (U).[34] Based on the properties of debris nano-fragments characterized in the present study and the other U occurrences within CsMPs,[5,9] we can surmise that at least three types of U occurrence that formed during the meltdown of the FDNPP reactors: (*i*) trace amounts of U were associated with Fe–Zn-oxide nanoparticles embedded in SiO_2 matrix within CsMP;[5] (*ii*) uraninite nanocrystals without detectable impurities, which were embedded within the Fe-oxide; *(iii)* eutectic U–Zr-oxide nanoparticles also formed. The type (*i*) U was described in detail in our previous studies.[5,9] The types (*ii*) and (*iii*) are the U occurrence the newly discovered phases described in this paper. The type (*i*) particles may be formed by volatilization of the partially oxidized fuels with low burnups and the volatilized U adsorbed onto Fe–Zn-oxide nanoparticles based on the $^{235}U/^{238}U$ isotope ratio greater than the average ratio calculated from the burnup.[9] Indeed, the hyperstoichiometric UO_{2+X} typically occurs during the meltdowns; X=0.03–0.14 in case of the TMI-2[28] and X = 0.23–0.42 in bore sample of PHEBUS FPT1 test.[30,35] Despite the evidence of

298 volatilization recorded in the CsMPs, the amount of molten fuels that have experienced
299 volatilization is likely to be small.[33] The existence of magnetite and uraninite phases is indicative
300 of the redox environment under accidental conditions: they appear to be more reducing than
301 oxidizing, probably due to the large quantities of metal present in the system (Fe, Zr).

302 Besides the nano-scale dimension, the compositions of the nano-fragments released from the
303 FDNPP, types (*ii*) and (*iii*), are comparable to those of the debris previously obtained from both
304 TMI-2 and Chernobyl.[27,32,36] In the present study, one of the U-rich particles (1 in Figure 4C,
305 Figure S5A) has pores with ~6 nm in size and defects; whereas, the Zr-rich particles (*e.g.*, 2 in
306 Figure 4C and E) have no pores, suggesting that U-Zr-oxide in the debris contains micron-sized
307 inclusion of gas phases, such as fissionogenic noble gases similar to those in irradiated fuels .[37]

308 The Nuclear Energy Agency[21,22] reported that elemental Fe is the dominant Fe phase in the
309 debris in the damaged reactors at the FDNPP, while magnetite should not be present or occur in
310 negligibly small amount based on the calculation. In contrast to their results, elemental Fe was
311 not characterized in the limited samples of the present study, although our results are consistent
312 with the last part of their conclusion. We do not propose that Fe oxide is dominant in the debris
313 but rather suggest that the occurrence of Fe-oxide is possible at the nano-scale with various
314 important features. The present study clearly reveals the presence of magnetite as a reactor debris
315 component and demonstrates the possible close association of uraninite as evidenced in AQC-A
316 and OTZ-A. Magnetite is also closely associated with Tc in the present samples (Figure 2G,
317 Figure S2 and S6). The Tc occurrence on the surface of magnetite and the encapsulation by the
318 CsMP exclude the possibility of magnetite formation as an alteration phase after release into the
319 environment. On the other hand, because ^{99}Tc is a fission product of major concern due to its
320 long half-life, 2.1×10^5 years[20] which is normally contained in fuel epsilon phase(s)[38] and with

small portions within the uraninite matrix, the occurrence of Tc in the debris is another issue that needs to be understood. Some Tc, which is classified as semi-volatile,[39] likely volatilized in the reactors and then was adsorbed and incorporated into the magnetite structure[40,41] during the FDNPP reactor unit meltdowns. Technetium can volatilize as oxidized forms at ~1200 K depending on the oxygen potential,[10] and the oxidation state of the Tc incorporated in the magnetite structure is likely to be Tc(IV), particularly when the other metals with low reducing potential were incorporated together[42] as detected in the present study. Since Fe phases, mostly Fe metal, are expected to occur as a major component of debris remaining in the damaged reactors, magnetite, which potentially forms at the surface of the Fe portion of the reactor debris, can contain not only uraninite but also other long-lived FPs, such as Tc.

The current status of debris in the damaged reactors was partially elucidated in the present study. Although the debris fragments are limited and extremely small, the physicochemical properties and the plausible formation processes give some insights to the partial properties of debris; in turn, this may provide useful information to the FDNPP decommissioning strategy. The gap between the evidence found in the present study and the results of the severe accident analysis code calculations,[21,22] such as the state of Fe speciation, strongly suggests the need for further detailed investigation on the debris, although it is extremely difficult to find the debris fragments in the environment. In addition, because several years have passed since the debris formed in the damaged reactors, the debris may be chemically altered due to contact with the injected water: first high-salinity seawater and later fresh water.[43] The instant release fraction (IRF) of the radionuclides that are unbound to debris matrix (estimated to be 5-10% of the total inventory) has already been leached from the corium.[33,44] Uraninite compounds in debris are known to dissolve relatively rapidly and to be controlled by surface interactions including oxidants

produced by the radiolysis of the water under oxidizing conditions, such as in the FDNPP, as compared with reducing conditions in a deep geologic repository.[33,45] Thus, precipitation of the secondary U phases over the debris surfaces and the retention of the other FP should be considered as it is in the alteration of spent nuclear fuels,[46] which are also constrained by the initial state of debris that was partially determined in the present study.

Environmental impacts of the released debris nano-fragments

The release of reactor debris fragments from the FDNPP into the surrounding environment has been, for the first time, explicitly revealed in the present study. The occurrence of debris fragments with intrinsic uraninite particles can greatly influence the mobility and bioavailability of the particle-associated radionuclides in ecosystem.[15] Remarkably, the CsMPs are an important medium for the transport of debris fragments in case of the FDNPP, although the possibility of the debris fragment released unassociated with CsMPs is also high. Because of the small size and association with CsMP, the mobility and stability of the reactor debris particles in Fukushima might be different from those of coarse fuel particles found in Chernobyl, which are constrained by the morphology and redox state.[47] However, the uraninite nanocrystals characterized in the present study were enwrapped by magnetite or CsMPs, suggesting that they are not presently in contact with the fluid. The dissolution of glassy CsMPs may initially proceed depending on the solution conditions similarly to the glass dissolution[48] and eventually expose the debris nano-fragments to fluids. Also, there is a high possibility of inhaling debris fragments along with CsMPs because the size of CsMPs associated with debris nano-fragments characterized in the present study is $< \sim 5\ \mu$m, which can reach to the deep respiratory system when inhaled.[49] Further work understanding the long-term behavior of FDNPP derived U particulates is now needed.

366

367

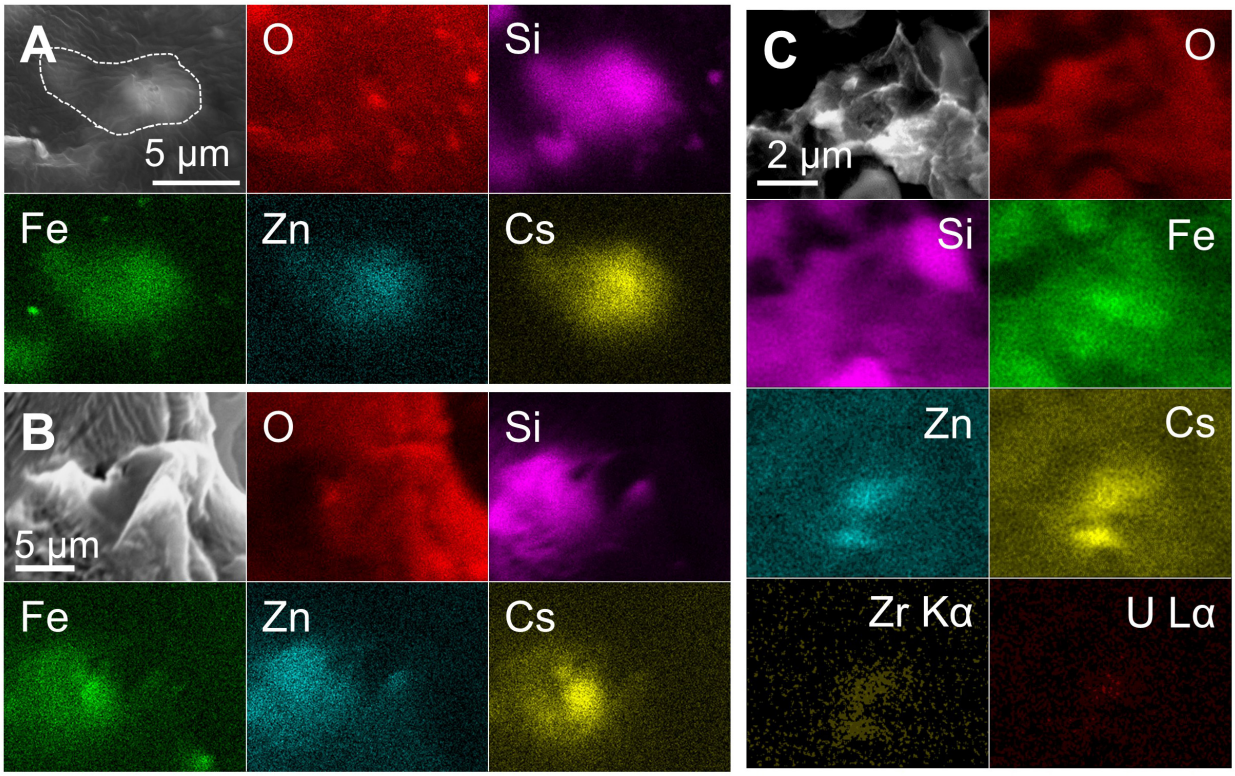

368

369 **Figure 1.** Secondary electron images of three CsMPs. (A) OTZ-A, (B) AQC-A and (C) OTZ-B,

370 and elemental maps of the major constituents obtained by SEM-EDX analysis.

371

372

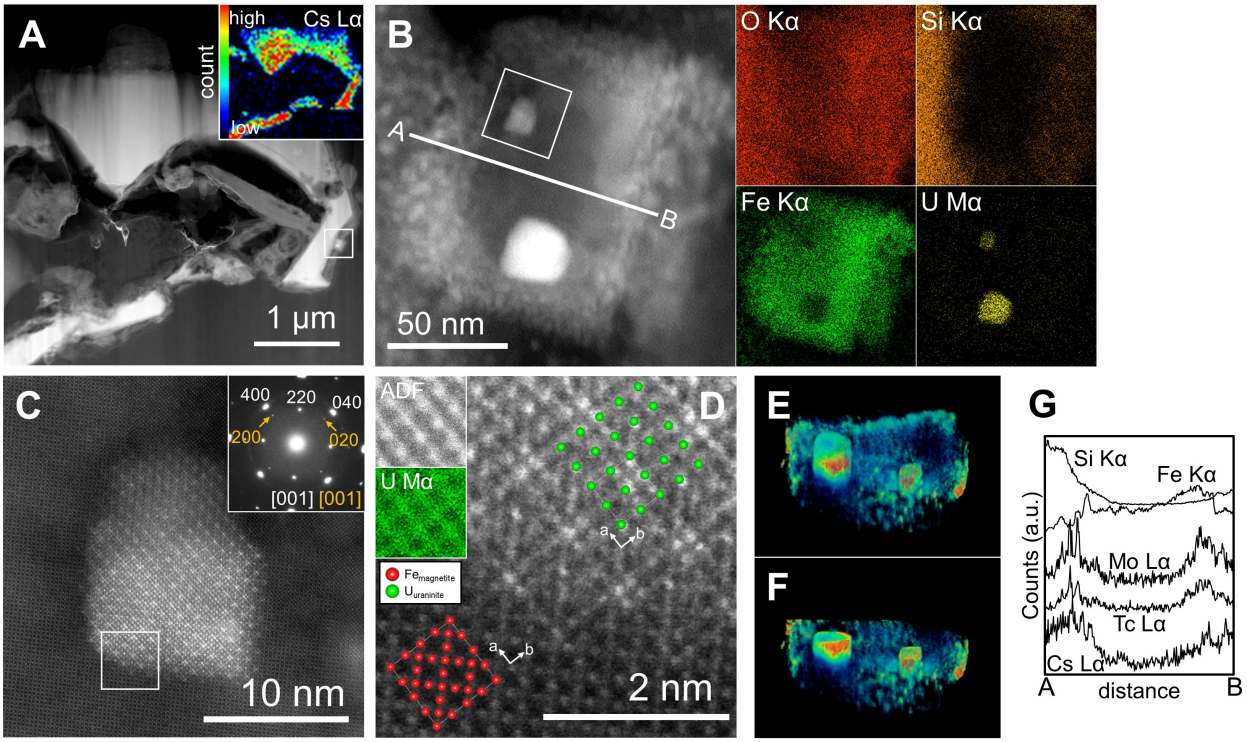

Figure 2. TEM characterization of the uraninite fragments in OTZ-A. (A) HAADF-STEM image of the half part of OTZ-A and the STEM-EDX map of Cs Lα, of which the color represents the X-ray counts. (B) HAADF-STEM image of the same Fe-U particle observed in Figure S1B after thinning by FIB, and the elemental maps of the selected elements. The white square and line segment AB are further characterized in Figure 2C and Figure 2G, respectively. (C) Magnified image of the area indicated by the white square in Figure 2B and the SAED pattern, which are collected from the area including both Fe oxide and U oxide nanoparticles. Indexes in white and yellow letters corresponds to magnetite and uraninite structures, respectively. The white square is further magnified in Figure 2D. (D) High-resolution HAADF-STEM image of the area indicated by the white square in Figure 2C. Fe atoms (red) of magnetite structure and U atoms (green) of uraninite structure are overlaid in the image. An atomic-column elemental map of U is also included. (E) Electron tomography showing the three-dimensional structure of uraninite nanoparticles in magnetite nanoparticle. See supplementary video file for further detail. (F) A

387 cross-sectional view of uraninite nanoparticles embedded with the magnetite nanoparticle. A part
388 of the euhedral rectangular shape can be observed, although the top and bottom of this magnetite
389 nanoparticle was removed by the FIB thinning. (G) STEM-EDX line-scan analysis of the
390 traverse AB in Figure 2B.

391

392

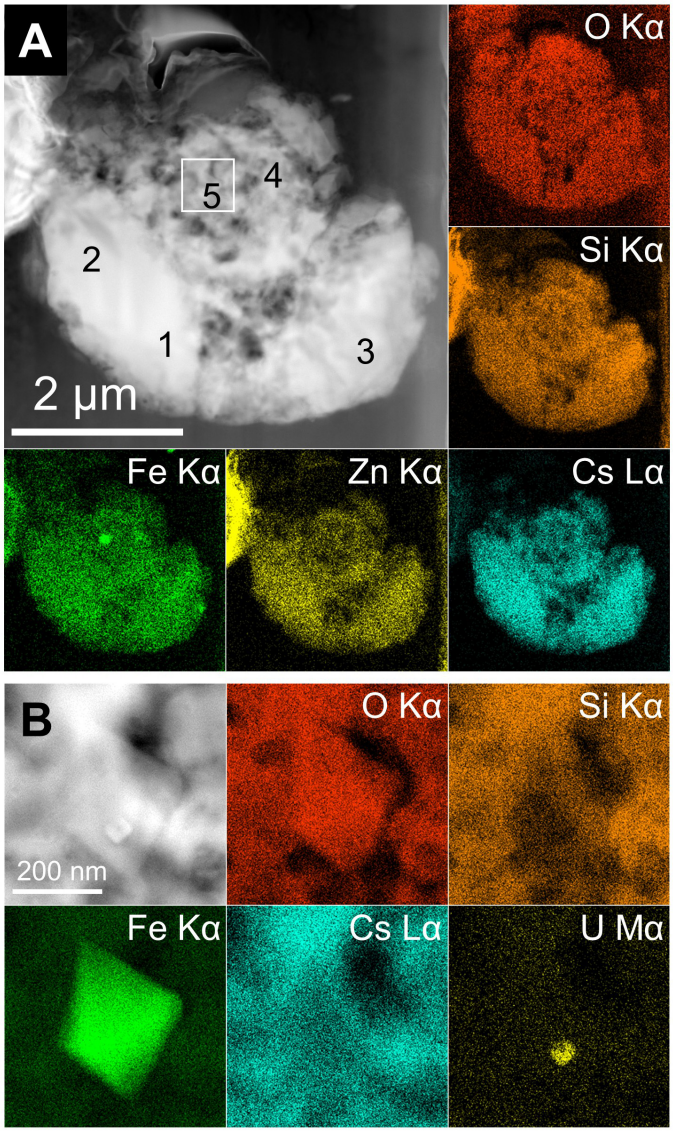

393

394 **Figure 3.** TEM characterization of the uraninite fragments in AQC-A. (A) HAADF-STEM
395 image of AQC-A and the elemental map of the major constituents. The numbers represents the
396 analytical points by STEM-EDX in Table 2. (B) Enlarged image of the area indicated by the
397 white square in Figure 3A associated with the elemental maps.

398

399

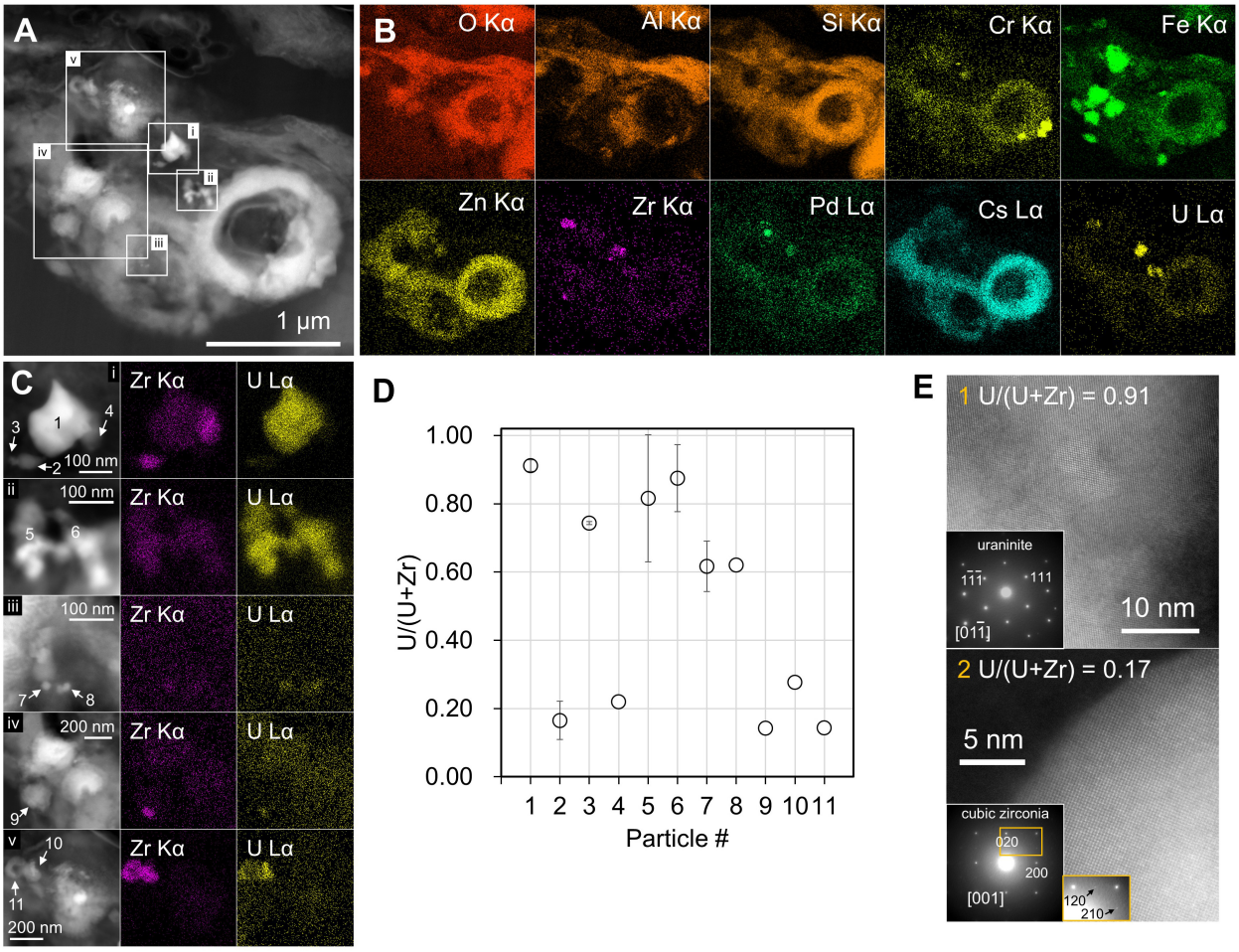

Figure 4. TEM characterization of the U–Zr oxide fragments in OTZ-B. (A) HAADF-STEM image of the aggregates of CsMPs in OTZ-B, where U–Zr oxide nanoparticles are present. (B) The elemental maps of major constituents in the Figure 4A. (C) Magnified HAADF-STEM images for the areas indicated by the white square with Roman numbers in Figure 4A associated with the elemental maps of Zr(Kα) and U(Lα). The Arabic numbers indicated by the arrows correspond to the particle numbers in Figure 4D. (D) The molar ratios of U/(U+Zr) analyzed using STEM-EDX. The ratios reveal the average values; n=7 for particle 1, n=5 for particle 2, and n=2 for particles 3, 5, 6 and 7, and n=1 for the others without error bar. The error bars show the standard deviations (2σ). (E) HR-HAADF-STEM images of U–Zr-oxides nanoparticles 1 and 2 in Figure 4C associated with the SAED patterns. U-rich particle 1 (U/(U+Zr) = 0.91) is

identified as uraninite structure, and Zr-rich particle 2 (U/(U+Zr) = 0.17) as cubic zirconia structure. The magnified SAED pattern with yellow frame is inserted for particle 2.

Supporting Information

Supplementary sections present ancillary STEM data and information on the radionuclide content of the CsMPs as determined by radiometric counting.

ASSOCIATED CONTENT

Figure S1. Results of STEM-EDX analysis of OTZ-A and the Fe-U oxide particle.

Figure S2. TEM results of uraninite nanoparticles embedded in magnetite nanoparticle associated with OTZ-A.

Figure S3. STEM-EDX analysis of OTZ-B.

Figure S4. Schematic illustration of zirconia structures (top panels) and the simulated SAED patterns viewed along [001] (bottom panels).

Figure S5. Results of STEM analysis of U–Zr oxide nanoparticle in OTZ-B.

Figure S6. Evidence of Tc occurrence in OTZ-B revealed by STEM-EDX analysis.

Table S1. Summary of the particle size, radioactivity and radioactivity ratio of OTZ-A, AQC-A and OTZ-B.

Table S2. Chemical composition (wt. %) of the area analysis on OTZ-A, AQC-A and OTZ-B as determined by STEM-EDX standardless analysis.

Movie S1. The three dimensional electron tomography of Fe-U particle in OTZ-A.

AUTHOR INFORMATION

Corresponding Author

*E-mail: utsunomiya.satoshi.998@m.kyushu-u.ac.jp

Author Contributions

S.U. conceived the idea, designed all experiments. A.O. conducted TEM analysis. A.O. and S. U. wrote the manuscript. J.I., M.S., T.K., G.F., and R.I. performed separation of CsMPs and SEM analysis. T.O. provided navigation during field research in Fukushima. S.Y. performed gamma spectroscopy at Tsukuba University. G.T.W.L, B.G., and R.C.E. participated in the discussion and interpretation of the results and helped to write the paper.

Notes

The authors declare no competing financial interests.

ACKNOWLEDGMENT

The authors are grateful to Dr. Watanabe for her assistance on SEM analyses at the Center of Advanced Instrumental Analysis, Kyushu University. This study is partially supported by JST Initiatives for Atomic Energy Basic and Generic Strategic Research and by a Grant-in-Aid for Scientific Research (KAKENHI) from the Japan Society for the Promotion of Science

(16K12585, 16H04634, No. JP26257402). SU is also supported by The Mitsubishi Foundation /Research Grants in the Natural Sciences and by ESPEC Foundation for Global Environment Research and Technology (Charitable Trust) (ESPEC Prize for the Encouragement of Environmental Studies). G. L acknowledges UK NERC funding (NE/M014088/1). The findings and conclusions of the authors of this paper do not necessarily state or reflect those of the JST.

REFERENCES

(1) Steinhauser, G.; Brandl, A.; Johnson, T. E. Comparison of the Chernobyl and Fukushima nuclear accidents: A review of the environmental impacts. *Sci. Total Environ.* **2014**, *470–471*, 800–817.

(2) Chino, M.; Nakayama, H.; Nagai, H.; Terada, H.; Katata, G.; Yamazawa, H. Preliminary Estimation of Release Amounts of 131 I and 137 Cs Accidentally Discharged from the Fukushima Daiichi Nuclear Power Plant into the Atmosphere. *J. Nucl. Sci. Technol.* **2011**, *48* (7), 1129–1134.

(3) Devell, L.; Johansson, K. *Specific Features of Cesium Chemistry and Physics Affecting Reactor Accident Source Term Predictions*; SKI Report 94:29, Swedish Nuclear Power Inspectorate: Stockholm, Sweden, 1994.

(4) Adachi, K.; Kajino, M.; Zaizen, Y.; Igarashi, Y. Emission of spherical cesium-bearing particles from an early stage of the Fukushima nuclear accident. *Sci. Rep.* **2013**, *3* (1), 2554.

(5) Furuki, G.; Imoto, J.; Ochiai, A.; Yamasaki, S.; Nanba, K.; Ohnuki, T.; Grambow, B.; Ewing, R. C.; Utsunomiya, S. Caesium-rich micro-particles: A window into the meltdown events at the Fukushima Daiichi Nuclear Power Plant. *Sci. Rep.* **2017**, *7*, 42731.

(6) *Nuclear Safety in Light Water Reactors: Severe Accident Phenomenology*; Sehgal, B. R., Ed.; Elsevier: Amsterdam, The Netherlands, 2012.

(7) Abe, Y.; Iizawa, Y.; Terada, Y.; Adachi, K.; Igarashi, Y.; Nakai, I. Detection of uranium and chemical state analysis of individual radioactive microparticles emitted from the Fukushima nuclear accident using multiple synchrotron radiation X-ray analyses. *Anal. Chem.* **2014**, *86* (17), 8521–8525.

(8) Kogure, T.; Yamaguchi, N.; Segawa, H.; Mukai, H.; Motai, S.; Akiyama-Hasegawa, K.; Mitome, M.; Hara, T.; Yaita, T. Constituent elements and their distribution in the radioactive Cs-bearing silicate glass microparticles released from Fukushima nuclear plant. *Microscopy* **2016**, *65* (5), 451–459.

(9) Imoto, J.; Ochiai, A.; Furuki, G.; Suetake, M.; Ikehara, R.; Horie, K.; Takehara, M.; Yamasaki, S.; Nanba, K.; Ohnuki, T.; et al. Isotopic signature and nano-texture of cesium-rich micro-particles: Release of uranium and fission products from the Fukushima Daiichi Nuclear Power Plant. *Sci. Rep.* **2017**, *7* (1), 5409.

(10) Hiernaut, J.-P.; Wiss, T.; Papaioannou, D.; Konings, R. J. M.; Rondinella, V. V. Volatile fission product behaviour during thermal annealing of irradiated UO_2 fuel oxidised up to U_3O_8. *J. Nucl. Mater.* **2008**, *372* (2–3), 215–225.

(11) Sakaguchi, A.; Steier, P.; Takahashi, Y.; Yamamoto, M. Isotopic compositions of ^{236}U and Pu isotopes in "Black Substances" collected from roadsides in Fukushima prefecture: Fallout from the Fukushima Dai-ichi Nuclear Power Plant Accident. *Environ. Sci. Technol.* **2014**, *48* (7), 3691–3697.

(12) Tokyo Electric Power Company (TEPCO) Website; http://www.tepco.co.jp/nu/fukushima-np/roadmap/2017/images2/d170727_08-j.pdf.

(13) Kuriny, V. D.; Ivanov, Y. A.; Kashparov, V. A.; Loshchilov, N. A.; Protsak, V. P.; Yudin, E. B.; Zhurba, M. A.; Parshakov, A. E. Particle-associated Chernobyl fall-out in the local and intermediate zones. *Ann. Nucl. Energy* **1993**, *20* (6), 415–420.

(14) Salbu, B.; Krekling, T. Characterisation of radioactive particles in the environment. *Analyst* **1998**, *123* (5), 843–850.

(15) Salbu, B.; Lind, O. C. Radioactive particles released to the environment from the Fukushima reactors-Confirmation is still needed. *Integr. Environ. Assess. Manag.* **2016**, *12* (4), 687–689.

(16) Nishihara, K.; Iwamoto, H.; Suyama, K. *Estimation of fuel compositions in Fukushima-Daiichi Nuclear Power Plant*; JAEA-Data/Code 2012-018, Japan Atomic Energy Agency: Ibaraki, Japan, 2012.

(17) Rey, A.; Utsunomiya, S.; Gimenez, J.; Casas, I.; de Pablo, J.; Ewing, R. C. Stability of uranium (VI) peroxide hydrates under ionizing radiation. *Am. Mineral.* **2009**, *94* (2–3), 229–235.

(18) Wechsler, B. A.; Lindsley, D. H.; Prewitt, C. T. Crystal structure and cation distribution in titanomagnetites ($Fe_{3-x}Ti_xO_4$). *Am. Mineral.* **1984**, *69*, 754–770.

(19) Wyckoff, R. W. G. *Crystal Structures Vol.1*; John Wiley: New York, 1963.

(20) Choppin, G. R.; Liljenzin, J.-O.; Rydberg, J. *Radiochemistry and Nuclear Chemistry*, 3rd Editio.; Butterworth-Heinemann: Woburn, MA, 2002.

(21) Nuclear Regulation Agency. *Benchmark study of the accident at the Fukushima Daiichi Nuclear Power Plant (BSAF Project) - Phase I summary report*; NEA/CSNI/R(2015)18, Nuclear Energy Agency: Boulogne-Billancourt, France, 2015.

(22) Nagase, F.; Gauntt, R. O.; Naito, M. Overview and outcomes of the OECD/NEA benchmark study of the accident at the Fukushima Daiichi Nuclear Power Station. *Nucl. Technol.* **2016**, *196* (3), 499–510.

(23) *CRC Handbook of Chemistry and Physics, 95th Edition*; Haynes, W. M., Lide, D. R., Bruno, T. J., Eds.; CRC Press, Taylor & Francis Group: Boca Raton, FL, 2014.

(24) Sanibondi, P. Numerical investigation of the effects of iron oxidation reactions on the fume formation mechanism in arc welding. *J. Phys. D. Appl. Phys.* **2015**, *48* (34), 345202.

(25) Jenkins, N. T.; Eagar, T. W. Chemical analysis of welding fume particles. *Weld. J.* **2005**, *84* (6), 87s–93s.

(26) Carpenter, K. R.; Monaghan, B. J.; Norrish, J. Analysis of fume formation rate and fume particle composition for Gas Metal Arc Welding (GMAW) of plain carbon steel using different shielding gas compositions. *ISIJ Int.* **2009**, *49* (3), 416–420.

(27) Olsen, C. S.; Jensen, S. M.; Carlson, E. R.; Cook, B. A. Materials interactions and temperatures in the Three Mile Island Unit 2 core. *Nucl. Technol.* **1989**, *87* (1), 57–94.

(28) Bottomley, P. D.; Coquerelle, M. Metallurgical examination of bore samples from the Three Mile Island Unit 2 reactor core. *Nucl. Technol.* **1989**, *87* (1), 120–136.

(29) Almjashev, V. I.; Barrachin, M.; Bechta, S. V.; Bottomley, D.; Defoort, F.; Fischer, M.; Gusarov, V. V.; Hellmann, S.; Khabensky, V. B.; Krushinov, E. V.; et al. Eutectic crystallization in the $Fe_{1.5}$–UO_{2+x}–ZrO_2 system. *J. Nucl. Mater.* **2009**, *389* (1), 52–56.

(30) Barrachin, M.; Chevalier, P. Y.; Cheynet, B.; Fischer, E. New modelling of the U–O–Zr phase diagram in the hyper-stoichiometric region and consequences for the fuel rod liquefaction in oxidising conditions. *J. Nucl. Mater.* **2008**, *375* (3), 397–409.

(31) Cohen, I.; Schaner, B. E. A metallographic and X-ray study of the UO_2-ZrO_2 system. *J. Nucl. Mater.* **1963**, *9* (1), 18–52.

(32) Brown, A.; McIntyre, G. J.; Gräslund, C. Analysis of crystalline phases in core bore materials from Three Mile Island Unit 2. *Nucl. Technol.* **1989**, *87* (1), 137–145.

(33) Grambow, B.; Poinssot, C. Interactions between nuclear fuel and water at the Fukushima Daiichi reactors. *Elements* **2012**, *8* (3), 213–219.

(34) Pontillon, Y.; Ducros, G.; Malgouyres, P. P. Behaviour of fission products under severe PWR accident conditions VERCORS experimental programme—Part 1: General description of the programme. *Nucl. Eng. Des.* **2010**, *240* (7), 1843–1852.

(35) Bottomley, P. D. W.; Brémier, S.; Papaioannou, D.; Walker, C. T. EPMA and X-Ray diffraction of the degraded fuel bundle from the Phebus FPT1 test. *Microchim. Acta* **2002**, *139* (1–4), 27–38.

(36) Shiryaev, A. A.; Vlasova, I. E.; Burakov, B. E.; Ogorodnikov, B. I.; Yapaskurt, V. O.; Averin, A. A.; Pakhnevich, A. V.; Zubavichus, Y. V. Physico-chemical properties of Chernobyl lava and their destruction products. *Prog. Nucl. Energy* **2016**, *92*, 104–118.

(37) Konings, R. J. M.; Wiss, T.; Beneš, O. Predicting material release during a nuclear reactor accident. *Nat. Mater.* **2015**, *14* (3), 247–252.

(38) Kleykamp, H. The chemical state of the fission products in oxide fuels. *J. Nucl. Mater.* **1985**, *131* (2–3), 221–246.

(39) Pontillon, Y.; Ducros, G. Behaviour of fission products under severe PWR accident conditions. The VERCORS experimental programme—Part 2: Release and transport of fission gases and volatile fission products. *Nucl. Eng. Des.* **2010**, *240* (7), 1853–1866.

(40) Marshall, T. A.; Morris, K.; Law, G. T. W.; Mosselmans, J. F. W.; Bots, P.; Parry, S. A.; Shaw, S. Incorporation and retention of 99-Tc(IV) in magnetite under high pH conditions. *Environ. Sci. Technol.* **2014**, *48* (20), 11853–11862.

(41) Kobayashi, T.; Scheinost, A. C.; Fellhauer, D.; Gaona, X.; Altmaier, M. Redox behavior of Tc(VII)/Tc(IV) under various reducing conditions in 0.1 M NaCl solutions. *Radiochim. Acta* **2013**, *101* (5), 323–332.

(42) Lee, M.-S.; Um, W.; Wang, G.; Kruger, A. A.; Lukens, W. W.; Rousseau, R.; Glezakou, V.-A. Impeding ^{99}Tc(IV) mobility in novel waste forms. *Nat. Commun.* **2016**, *7*, 12067.

(43) Burns, P. C.; Ewing, R. C.; Navrotsky, A. Nuclear fuel in a reactor accident. *Science* **2012**, *335* (6073), 1184–1188.

(44) Ferry, C.; Piron, J.-P.; Poulesquen, A.; Poinssot, C. Radionuclides release from the spent fuel under disposal conditions: Re-evaluation of the instant release fraction. *MRS Proc.* **2008**, *1107*, 447.

(45) Ewing, R. C. Long-term storage of spent nuclear fuel. *Nat. Mater.* **2015**, *14* (3), 252–257.

(46) Burns, P. C.; Klingensmith, A. L. Uranium mineralogy and neptunium mobility. *Elements* **2006**, *2* (6), 351–356.

(47) Salbu, B.; Janssens, K.; Lind, O. C.; Proost, K.; Gijsels, L.; Danesi, P. R. Oxidation states of uranium in depleted uranium particles from Kuwait. *J. Environ. Radioact.* **2004**, *78* (2), 125–135.

(48) Hellmann, R.; Cotte, S.; Cadel, E.; Malladi, S.; Karlsson, L. S.; Lozano-Perez, S.; Cabié, M.; Seyeux, A. Nanometre-scale evidence for interfacial dissolution–reprecipitation control of silicate glass corrosion. *Nat. Mater.* **2015**, *14* (3), 307–311.

(49) *Air Quality Criteria for Particulate Matter Volume II*; EPA/600/P-99/002bF, United States Environmental Protection Agency, National Center for Environmental Assessment: NC, 2004.